

An Effective Membership Probability Representation for Point Set Registration

LU-JIE FANG¹, ZHAN-LI SUN¹, (Member, IEEE),
AND KIN-MAN LAM², (Senior Member, IEEE)

¹School of Electrical Engineering and Automation, Anhui University, Hefei 230601, China

²Department of Electronic and Information Engineering, The Hong Kong Polytechnic University, Hong Kong

Corresponding author: Zhan-Li Sun (zhlsun2006@126.com)

This work was supported by the National Natural Science Foundation of China under Grant 61972002.

ABSTRACT How to design an effective membership probability is an important component for Gaussian mixture model (GMM) of point set registration. In order to improve the robustness of point set registration, in this paper, a new representation is proposed for membership probability of Gaussian mixture model, by utilizing two types of feature descriptor, i.e. shape context or fast point feature histograms. Moreover, for each point of the model point set, a dynamic programming (DP) algorithm is developed to search for the optimal candidate points from the target point set. Compared to the state-of-the-art approaches, the proposed approach is more robust to deformation, outlier, occlusion, and rotation. Experimental results on several widely used 2D and 3D data demonstrate the effectiveness and feasibility of the proposed algorithm.

INDEX TERMS Gaussian mixture model, point set registration, dynamic programming.

I. INTRODUCTION

The task of point set registration is to find an optimal spatial transformation to align a model point set and a target point set. As a key component in computer vision, point set registration have been widely used in numerous applications, e.g., shape matching [1], visual navigation [2], stereo system [3], [4], image registration [5], defect detection [6], etc.

So far, many algorithms have been developed for point set registration. Due to its simplicity and low computational complexity, iterative closest point (ICP) was probably the most classical approach, by utilizing the nearest-neighbor relationship to assign a binary correspondence at each step [7]. However, the performance of ICP degenerates quickly for data with outliers and large deformations. In [8], the thin-plate spline was used as the parameterization of non-rigid spatial mapping. Moreover, instead of a strictly binary correspondence, the softassign was introduced in [8] for the correspondence to improve the robustness. In [9], an asymmetric point matching (APM) algorithm [9] was proposed to formulate

the matching problem as a concave quadratic assignment problem, by eliminating the transformation variables of [8].

The feature-based non-rigid registration is an important branch of point set registration. In [10], a descriptor, shape context (SC), was proposed to provide a globally discriminative characterization for shape matching. The shape context at a reference point captures the distribution of the remaining points relative to it. A local spectral descriptor was proposed in [11] to represent the attribute domain of feature points. For a point in a given point-set, the weight graphs are constructed based on its neighboring points. In [12], two distance features were defined for measuring global and local structural differences between two point sets, respectively. Kernel correlation, a very effective way to align intensity images, was extended to point set registration [13], [14].

As an effective model, Gaussian mixture model (GMM) has been widely applied on point set registration. For this kind of methods, the discrete point sets are represented via GMM. On the one hand, the point set can be interpreted as statistical samples, which are drawn from a continuous probability distribution of random point locations. This interpretation explicitly reflects the uncertainty of the extraction process of the point sets to be registered. On the other hand,

The associate editor coordinating the review of this manuscript and approving it for publication was Chunbo Xiu.

the traditionally hard discrete optimization problems can be potentially converted to more tractable continuous optimization problems by means of GMM [15]. A probabilistic method, called the coherent point drift (CPD) algorithm, was proposed in [16] for both rigid and nonrigid point set registration. In CPD, the GMM centroids, i.e. the model point set, were fitted to the target point set by maximizing the likelihood. For GMM, how to design an effective membership probability is an important component for point set registration. In [16], for simplicity, the membership probabilities were assumed to be equal for all GMM components. Nevertheless, the CPD algorithm was sensitive to outliers and occlusion. In [17], the correspondences between two point sets were obtained by matching their feature descriptors, and then used to initialize the membership probabilities according to two rules.

In our work, a new representation is proposed for membership probability of Gaussian mixture model. Different from [17], for the unmatched points, the membership probabilities are devised by considering the feature descriptor distance, instead of a constant. Dynamic programming (DP) is a powerful technique for discrete optimization problem. The DP algorithm decomposes an original problem into several subproblem. Different from classical recursive methods, the solution of each subproblem is saved and used multiple times for solving larger subproblems [18]. Since the whole solution of DP algorithm satisfies the optimal solution of the subset, the DP algorithm can better maintain the substructure. In our work, for each point of the model point set, a dynamic programming algorithm is developed to search for the optimal candidate points from the target point set.

The main contributions of the work can be summarized as two aspects: (a) An effective membership probability is devised for Gaussian mixture model by means of the feature descriptor distance. (b) Given the membership probability representation, a dynamic programming algorithm is developed to search for the optimal candidate points.

The remainder of the paper is organized as follows. A detailed description of the proposed method is presented in Section II. Experimental results are given in Section III. Finally, conclusions are made in Section IV.

II. METHODOLOGY

A. GAUSSIAN MIXTURE MODEL

Assume that there are two point sets, N model points $\mathbf{X} = [\mathbf{x}_1, \mathbf{x}_2, \dots, \mathbf{x}_N]^T$ and M target points $\mathbf{Y} = [\mathbf{y}_1, \mathbf{y}_2, \dots, \mathbf{y}_M]^T$ in D -dimensional space. The goal of point set registration is to estimate a transformation $T(\mathbf{X})$ to wrap the model point set \mathbf{X} to the target point set \mathbf{Y} .

Considering $T(\mathbf{X})$ as the centroids, the target points can be drawn according to the following Gaussian mixture model,

$$P(\mathbf{y}_m|\boldsymbol{\theta}) = \gamma \frac{1}{a} + (1 - \gamma) \sum_{n=1}^N \frac{C_{mn}}{(2\pi\sigma^2)^{D/2}} e^{-\frac{\|\mathbf{y}_m - T(\mathbf{x}_n)\|^2}{2\sigma^2}}, \quad (1)$$

where σ^2 is the variance of the Gaussian distribution, C_{mn} denotes the membership probability of Gaussian mixture model, a is a constant, and γ is the percentage of outliers [16]. For GMM, the unknown parameter vector $\boldsymbol{\theta} = \{T, \sigma^2, \gamma\}$ can be obtained by minimizing the following negative log-likelihood function,

$$\begin{aligned} E(\boldsymbol{\theta}) &= - \sum_{m=1}^M \ln P(\mathbf{y}_m|\boldsymbol{\theta}) \\ &= \frac{1}{2\sigma^2} \sum_{m=1}^M \sum_{n=1}^N P(n|\mathbf{y}_m, \boldsymbol{\theta}^{old}) \|\mathbf{y}_m - T(\mathbf{x}_n)\|^2 \\ &\quad + \frac{M_{\mathbf{P}}D}{2} \ln \sigma^2 - M_{\mathbf{P}} \ln(1 - \gamma) - (M - M_{\mathbf{P}}) \ln \gamma \\ &\quad + \frac{\lambda}{2} \phi(\mathbf{v}), \end{aligned} \quad (2)$$

where $\boldsymbol{\mu}^{old}$ denotes the current parameter values [16], and

$$M_{\mathbf{p}} = \sum_{m=1}^M \sum_{n=1}^N P(n|\mathbf{y}_m, \boldsymbol{\mu}^{old}) \leq M. \quad (3)$$

In (2), $\phi(\mathbf{v})$ is a coherent constraint,

$$\phi(\mathbf{v}) = \text{tr}(\mathbf{W}^T \mathbf{G} \mathbf{W}), \quad (4)$$

where \mathbf{W} is a matrix of coefficients, \mathbf{G} is a kernel matrix, and $\text{tr}(\cdot)$ denotes the trace [16].

B. MEMBERSHIP PROBABILITY REPRESENTATION

1) MEMBERSHIP PROBABILITY REPRESENTATION BASED ON FEATURE DESCRIPTOR

In the proposed approach, the membership probability C_{mn} in (1) is devised based on two types of feature descriptor, i.e. shape context (SC) [10] and fast point feature histograms (FPFH) [19], for 2D and 3D data, respectively. As a globally discriminative characterization, the SC at a reference point can capture the distribution of the remaining points relative to it. For shape context, all measurements are taken with respect to points on the object. Thus, shape context is more robust to rotation, scale variation, occlusion, and outlier. FPFH can effectively represent the underlying surface model properties at a point. As a local feature, FPFH provides an overall scale and pose invariant multi-value feature in 3D point set registration.

For SC, the whole 2D plane is first divided into some uniform bins in log-polar space, in order to make the descriptor more sensitive to positions of nearby sample points than to those of points farther away [10]. For a point \mathbf{x}_i , a histogram $h_i(k)$ of the k th bin can be defined according to the distance to the remaining points \mathbf{x}_j , i.e.,

$$h_i(k) = \#\{(\mathbf{x}_j - \mathbf{x}_i) \in \text{bin}(k), j \neq i\} \quad (5)$$

For a reference point \mathbf{x}_i , the point feature histogram (PFH) can be computed in two steps [19]. First, the points in a sphere with a given radius r are selected as the neighbors of \mathbf{x}_i . Then, three angular variations are computed between the normals of

\mathbf{x}_i and each neighbor \mathbf{x}_j . The Euclidean distance between \mathbf{x}_i and \mathbf{x}_j , together with three angular variations, are merged as a histogram $h_i(k)$.

Consider two points, the point n in the model point set and the point m in the target point set, the feature descriptor based histograms are represented as $h_n(k)$ and $h'_m(k)$ ($k = 1, 2, \dots, K$), respectively [10]. The feature descriptor distance $V(m, n)$ between two points can be computed as,

$$V(m, n) = \frac{1}{2} \sum_{k=1}^K \frac{[h_n(k) - h'_m(k)]^2}{h_n(k) + h'_m(k)}. \quad (6)$$

Given $V(m, n)$, the membership probability C_{mn} of GMM can be defined as,

$$C_{mn} = \begin{cases} \rho_1 * \max(V_{mn}), & \text{if } m = t_n, \\ e^{-\rho_2 / V_{mn}}, & \text{if } m \neq t_n, \end{cases} \quad (7)$$

where ρ_1 and ρ_2 are two constants, (t_1, t_2, \dots, t_N) refer to the optimal candidate points that assign point y_{t_n} in target point set to point x_n in model point set.

For simplicity, in [16], the membership probabilities are set to be equal, i.e., $P(M) = \frac{1}{M}$, for all GMM components. In [17], if a data point \mathbf{y}_m does not have a corresponding model point, the equal membership probabilities are set for all GMM components. As shown in (7), the soft membership probabilities are devised to the unmatched points, by considering the local shape distances $V(m, n)$.

2) CANDIDATE SEARCH WITH DP ALGORITHM

In stead of search for the optimal candidate points (t_1, t_2, \dots, t_N) via finding the minimal feature descriptor distance $V(m, n)$ [17], a DP algorithm is devised in order to keep up the spatial structure of neighbor points [18]. A natural energy function for DP can be defined as,

$$\min \sum_{i=1}^j V(t_i, i), \quad j = N, N-1, \dots, 1. \quad (8)$$

A set of optimal candidate points (t_1, t_2, \dots, t_N) can be searched one by one, by minimizing the energy function in (8). First, a minimum operation is defined for three input variables a, b , and c , i.e.,

$$L(m, n) = \begin{cases} 1, & \text{if } \min(a, b, c) = a, \\ 2, & \text{if } \min(a, b, c) = b, \\ 3, & \text{if } \min(a, b, c) = c, \end{cases} \quad (9)$$

Furthermore, an auxiliary matrix $\mathbf{B} \in R^{M \times N}$ is derived through the following recursive equations,

$$\mathbf{B}(1, 1) = \min (V(1, 1), \tau), \quad (10)$$

$$\mathbf{B}(m, 1) = \min (\mathbf{B}(m-1, 1) + \tau, V(m, 1) + \tau * (m-1)), \\ m = 2, 3, \dots, M, \quad (11)$$

$$\mathbf{B}(1, n) = \min (\mathbf{B}(1, n-1) + \tau, V(1, n) + \tau * (n-1)), \\ n = 2, 3, \dots, N, \quad (12)$$

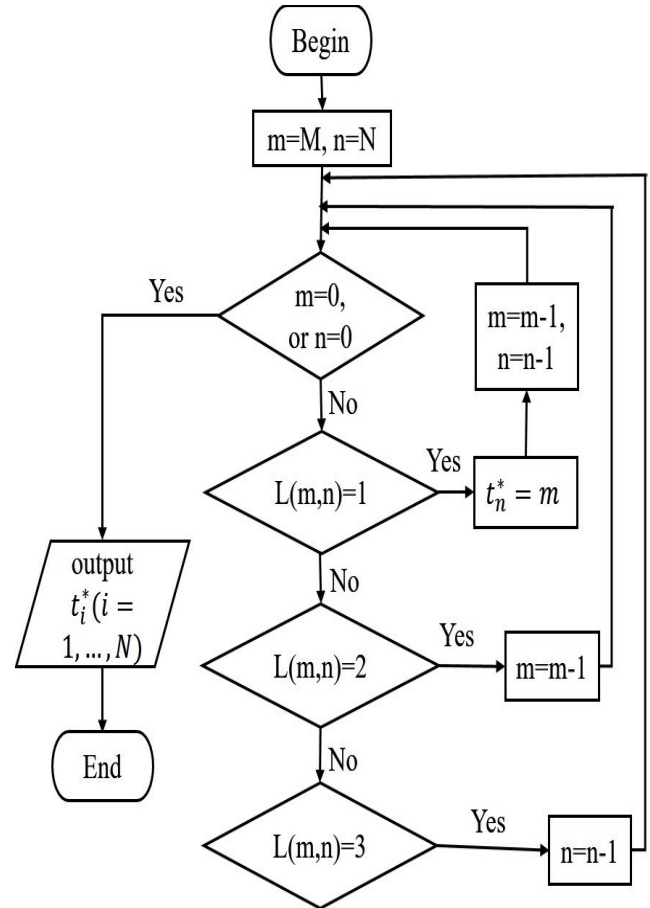


FIGURE 1. Flowchart of the search process of the optimal candidate points (t_1, t_2, \dots, t_N) according to the auxiliary matrix \mathbf{L} .

$$\mathbf{B}(m, n) = \min (\mathbf{B}(m-1, n-1) + V(m, n), \\ \mathbf{B}(m-1, n) + \tau, \mathbf{B}(m, n-1) + \tau), \\ m = 2, 3, \dots, M, n = 2, 3, \dots, N, \quad (13)$$

where τ is a given threshold [18]. In terms of (9), we can obtain the values of $L(m, n)$ corresponding to (10)-(13). Furthermore, the optimal candidate points (t_1, t_2, \dots, t_N) can be determined by,

$$\begin{cases} \text{if } L(m, n) = 1, & t_n^* = m, m = m-1, n = n-1, \\ \text{if } L(m, n) = 2, & m = m-1, \\ \text{if } L(m, n) = 3, & n = n-1, \end{cases} \quad (14)$$

For (14), Fig. 1 shows the flowchart of the search process of the optimal candidate points (t_1, t_2, \dots, t_N) according to the auxiliary matrix \mathbf{L} .

C. THE EM ALGORITHM

The unknown variables in (2) are solved through the the EM algorithm. The optimization process is alternated between two steps: an expectation step (E-step) and a maximization step (M-step) [17].

Algorithm 1 The Proposed Algorithm

- 1: Input: model point set \mathbf{X} , target point set \mathbf{Y} ;
- 2: Output: nonrigid transformation $T(\mathbf{X})$, and correspondence matrix \mathbf{P} ;
- 3: Initialize: weighting coefficients $\lambda, \gamma, \beta, \mathbf{W} = \mathbf{0}, \sigma^2 = \frac{1}{DMN} \sum_{m,n=1}^{M,N} \|\mathbf{y}_m - \mathbf{x}_n\|^2$;
- 4: **repeat**
- 5: E-step:
- 6: Compute C_{mn} by (7);
- 7: Update \mathbf{P} by (15);
- 8: M-step:
- 9: Compute \mathbf{W} by (18);
- 10: Update $f(\mathbf{X}) = \mathbf{X} + \mathbf{G}\mathbf{W}$;
- 11: Calculate γ and σ^2 by (16) and (17), respectively;
- 10: **until** converges;
- 11: The transformation $f(\mathbf{X}) = \mathbf{X} + \mathbf{G}\mathbf{W}$ and the optimal correspondence matrix \mathbf{P} .

1) EXPECTATION STEP

After deriving the membership probability according to the method in Section II-B, the posterior probabilities p_{mn} of GMM components can be computed as,

$$p_{mn} = \frac{C_{mn} e^{-\frac{\|\mathbf{y}_m - T(\mathbf{x}_n)\|^2}{2\sigma^2}}}{\sum_{k=1}^N C_{mk} e^{-\frac{\|\mathbf{y}_m - T(\mathbf{x}_k)\|^2}{2\sigma^2}} + \frac{\gamma(2\pi\sigma^2)^{(D/2)}}{(1-\gamma)^2}} \quad (15)$$

2) MAXIMIZATION STEP

After obtaining P , we compute the partial derivatives of (2) with respect to γ, σ^2 and \mathbf{W} , and set them as zeros [17]. We can obtain,

$$\gamma = 1 - \frac{M\mathbf{P}}{M} \quad (16)$$

$$\sigma^2 = \frac{\sum_{m=1}^M \sum_{n=1}^N p_{mn} \|\mathbf{y}_m - T(\mathbf{x}_n)\|^2}{M\mathbf{P}D} \quad (17)$$

$$\mathbf{W} = (\mathbf{G} + \lambda\sigma^2 d(\mathbf{P}\mathbf{1})^{-1})^{-1} \times (d(\mathbf{P}\mathbf{1})^{-1} \mathbf{P}\mathbf{X} - \mathbf{Y}) \quad (18)$$

where $d(\cdot)^{-1}$ is the inverse diagonal matrix.

The process of proposed algorithm can be outlined in Algorithm 1.

III. EXPERIMENTAL RESULTS

A. EXPERIMENTAL DATA AND SET-UP

To evaluate the effectiveness of the proposed dynamic programming based membership probability method, denoted as DP-MP, we present the experimental comparisons to six state-of-the-art algorithms, including MSTT [20], APM [9], CPD [16], PRGLS [17], SCGF [21] and MR [22], [23]. All simulations were conducted in the Matlab environment, running on an ordinary personal computer with dual 3.0-GHz CPUs and 4-GB memory. In experiments, three types of data, i.e., synthetic data from *fish* and a Chinese character *Fu* [8], three sets of data with arbitrary shape [8], three sets

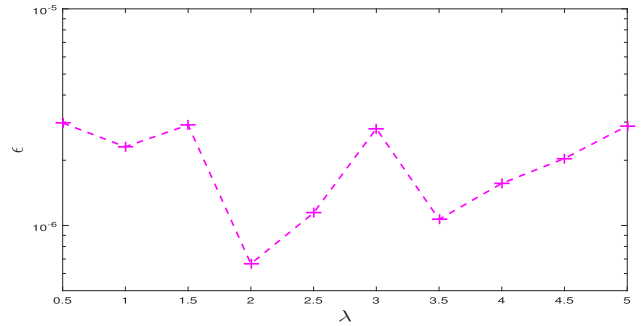


FIGURE 2. The registration errors of the *Fu* point sets when the weighting coefficient λ is set as different value.

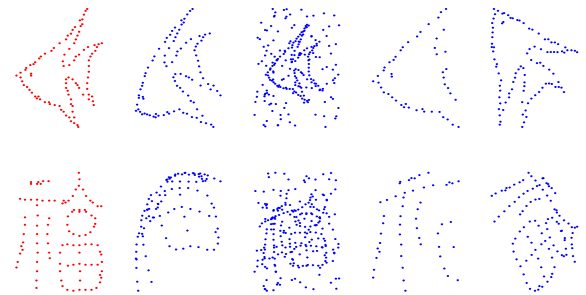


FIGURE 3. Model points of (left column) and their corresponding target points including deformation, outlier, occlusion and rotation (column 2 to 5).

of 3D face image sequences [16], [24], [25], are used to investigate the robustness of the various algorithms.

The registration error ϵ between the transformed model points $f(\mathbf{X})$ and the corresponding target points \mathbf{Y} [21], i.e.,

$$\epsilon = \left(\frac{\sum (\|f(\mathbf{X}) - \mathbf{Y}\|^2)}{N} \right)^{\frac{1}{2}} \quad (19)$$

is used to evaluate the registration accuracy.

As an example, Fig. 2 shows the registration errors of the point set *Fu* when the weighting coefficient λ is set as different value. We can see that the registration error fluctuates with the variation of λ . Therefore, it is necessary to determine the optimal weighting coefficient. Nevertheless, there is no a separated training procedure for point set registration. Traditional methods, such as cross validation, cannot be employed to choose the optimal parameters. In experiments, the grid search is adopted to find the approximately optimal parameter values for the weighting coefficients of the various methods.

B. EXPERIMENTAL COMPARISONS

1) EXPERIMENTAL RESULTS ON THE SYNTHETIC DATA

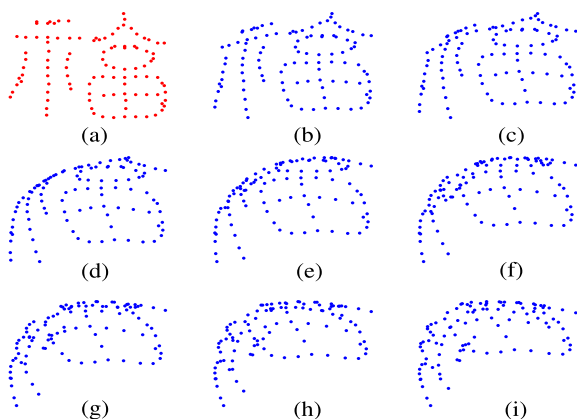
Two widely used shapes, a fish with 98 points and a Chinese character *Fu* with 105 points, are adopted as the model point sets, to produce the target point sets by adding deformation, outliers, occlusion and rotation. Figure 3 shows some examples of model points (*fish* and *Fu*) and their corresponding target points with deformation, outlier, occlusion and rotation, respectively.

TABLE 1. The mean and standard deviation ($\mu \pm \sigma$) of the registration errors of seven methods when the deformation parameter β is set as different value for the *fish* point sets.

β	0.04	0.06	0.08	0.10	0.12
MSTT	0.0017±0.0011	0.0055±0.0095	0.0115±0.0122	0.0147±0.0134	0.0218±0.0135
APM	0.0015±0.0009	0.0023±0.0014	0.0033±0.0019	0.0042±0.0026	0.0053±0.0032
CPD	1.2169e-6±9.2278e-7	1.4244e-6±1.1382e-6	9.9335e-5±1.8989e-4	2.8533e-4±3.7201e-4	0.0014±0.0025
PR-GLS	1.1890e-6±8.4312e-7	2.5694e-6±3.4274e-6	1.2952e-6±6.2102e-7	2.3159e-6±2.6854e-6	2.9618e-6±3.5699e-6
SCGF	2.2301e-4±2.8584e-4	3.3190e-4±2.4027e-4	3.0682e-4±2.0168e-4	5.8624e-4±6.7893e-4	6.9989e-4±4.6793e-4
MR	1.3849e-5±1.8468e-5	4.2672e-5±4.9457e-5	1.4493e-4±1.9982e-4	4.7160e-4±6.8501e-4	9.1741e-4±1.1741e-3
DP-MP	1.0133e-6±9.6902e-7	1.2779e-6±9.4786e-7	1.3759e-6±8.6305e-7	1.8630e-5±5.4812e-5	2.7589e-5±8.1569e-5
β	0.14	0.16	0.18		
MSTT	0.0255±0.0133	0.0258±0.0132	0.0328±0.0180		
APM	0.0064±0.0040	0.0080±0.0041	0.0097±0.0049		
CPD	0.0027±0.0039	0.0039±0.0040	0.0056±0.0049		
PR-GLS	4.6936e-5±1.4174e-4	9.0816e-5±2.8053e-4	0.0015±0.0036		
SCGF	0.0013±0.0010	0.0020±0.0016	0.0023±0.0017		
MR	0.0013±0.0014	0.0016±0.0013	0.0020±0.0017		
DP-MP	7.5869e-5±2.3404e-4	1.7895e-4±5.5639e-4	0.0018±0.0046		

TABLE 2. The mean and standard deviation ($\mu \pm \sigma$) of the registration errors of seven methods when the deformation parameter β is set as different value for the Chinese character *Fu*.

β	0.04	0.06	0.08	0.10	0.12
MSTT	0.0027±0.0015	0.0064±0.0043	0.0125±0.0137	0.0149±0.0149	0.0206±0.0165
APM	0.0023±0.0015	0.0036±0.0023	0.0059±0.0048	0.0075±0.0060	0.0098±0.0065
CPD	1.5180e-6±1.0949e-6	2.1225e-6±2.1141e-6	8.0008e-4±1.5135e-3	0.0033±0.0059	0.0077±0.0133
PR-GLS	1.6778e-4±2.8677e-4	6.9187e-4±9.1076e-4	0.0018±0.0026	0.0040±0.0044	0.0072±0.0071
SCGF	5.7185e-4±5.5625e-4	3.4065e-4±1.4750e-4	9.8019e-4±9.0890e-4	0.0010±0.0010	0.0019±0.0022
MR	2.3091e-5±2.6242e-5	1.2691e-4±1.6225e-4	0.0012±0.0018	0.0018±0.0017	0.0028±0.0025
DP-MP	1.0456e-6±8.0857e-7	1.1872e-6±9.4543e-7	1.9412e-6±9.7822e-7	2.0353e-6±1.1235e-6	2.3445e-6±1.0856e-6
β	0.14	0.16	0.18		
MSTT	0.0233±0.0165	0.0321±0.0181	0.0417±0.0202		
APM	0.0126±0.0088	0.0153±0.0103	0.0173±0.0112		
CPD	0.0100±0.0147	0.0176±0.0172	0.0193±0.0185		
PR-GLS	0.0110±0.0071	0.0162±0.0106	0.0196±0.0120		
SCGF	0.0020±0.0013	0.0025±0.0025	0.0029±0.0016		
MR	0.0042±0.0029	0.0051±0.0024	0.0065±0.0017		
DP-MP	3.2701e-6±2.0601e-6	2.2939e-6±1.2561e-6	2.9237e-6±2.3544e-6		

**FIGURE 4.** The model point set (a) and the wrapped point sets when the deformation parameter β is varied from 0.04 (b) to 0.18 (i) for the Chinese character *Fu*.

Referring to [20], non-rigid deformation was generated by means of the random data sampled from the standard normal distribution. The deformation parameter β is varied from 0.04 to 0.18 to change the deformation extent. As an example, Fig. 4 shows the model point set (a) and the wrapped

point sets when the deformation parameter β is varied from 0.04 (b) to 0.18 (i) for the Chinese character *Fu*. It can be seen that the point set has a larger deformation when β is increased. For each β , the random data are sampled ten times to obtain ten sets of synthetic data points. After ten trials, we compute the mean and standard deviation ($\mu \pm \sigma$) of the registration errors ϵ of ten sets of data.

Tables 1 and 2 show the mean and standard deviation ($\mu \pm \sigma$) of the registration errors of seven methods, when the deformation parameter β is set at different values. The best result and the second-best result are highlighted as red and blue, respectively. For the shape *fish*, the registration errors of DP-MP and PR-GLS are lower than that of other methods. For the shape *Fu*, the registration errors of DP-MP are lower than that of other methods, including PR-GLS. From Fig. 3, we can see that the topology structure of *fish* is relative simpler than that of *Fu*. As the topology structure of *fish* is simple, the target point set can also be well matched via the membership probability of PR-GLS. Therefore, compared to PR-GLS, the gain of performance improvement is not obvious for the shape *fish*. Nevertheless, for the shape *Fu*, the adjacent points may be wrongly matched when a deformation is

TABLE 3. The mean and standard deviation ($\mu \pm \sigma$) of the registration errors of seven methods when the outlier percentage P_o is set as different value for the fish point sets.

P_o	0.6	0.8	1.0	1.2	1.4
MSTT	0.0049±0.0104	0.0017±0.0011	0.0049±0.0106	0.0017±0.0012	0.0016±0.0010
APM	0.0048±0.0013	0.0051±0.0008	0.0064±0.0009	0.0067±0.0009	0.0063±0.0011
CPD	0.0010±0.0014	0.0039±0.0011	0.0054±0.0018	0.0059±0.0015	0.0073±0.0017
PR-GLS	7.6664e-5±1.7344e-4	5.5753e-4±5.1919e-4	4.2144e-4±5.4489e-4	0.0012±0.0016	0.0030±0.0033
SCGF	1.3434e-4±7.1958e-5	1.5676e-4±1.4607e-4	2.4696e-4±3.2489e-4	1.9242e-4±2.5764e-4	3.0803e-4±3.1880e-4
MR	7.6110e-5±1.1492e-4	1.4657e-4±1.9519e-4	3.1441e-4±3.7916e-4	3.6689e-4±2.5637e-4	7.0200e-4±6.0338e-4
DP-MP	1.3714e-6±1.2833e-6	1.3260e-6±1.0222e-6	2.0537e-6±9.6894e-7	1.2801e-6±8.4070e-7	2.0453e-6±1.6463e-6

TABLE 4. The mean and standard deviation ($\mu \pm \sigma$) of the registration errors of seven methods when the outlier percentage P_o is set as different value for the Chinese character Fu.

P_o	0.6	0.8	1.0	1.2	1.4
MSTT	0.0027±0.0015	0.0032±0.0023	0.0028±0.0015	0.0030±0.0018	0.0026±0.0016
APM	0.0073±0.0021	0.0080±0.0019	0.0078±0.0025	0.0095±0.0020	0.0093±0.0027
CPD	9.5997e-4±1.7598e-3	0.0036±0.0022	0.0052±0.0028	0.0054±0.0017	0.0061±0.0025
PR-GLS	6.9100e-5±2.1374e-4	3.8772e-5±1.1842e-4	3.1964e-4±6.1750e-4	3.5401e-4±6.7345e-4	2.7054e-4±8.5162e-4
SCGF	4.9608e-4±3.9469e-4	3.6181e-4±2.1340e-4	5.3792e-4±5.2190e-4	5.7710e-4±3.5997e-4	5.5075e-4±3.2354e-4
MR	1.2134e-4±8.9824e-5	8.3694e-4±9.7940e-4	0.0010±4.8199e-4	0.0014±7.5905e-4	0.0015±9.4710e-4
DP-MP	1.2259e-6±7.3526e-7	1.5629e-6±9.1148e-7	1.5090e-6±1.0221e-6	2.0958e-6±1.1382e-6	1.5471e-6±1.3852e-6

happened. Thus, compared to PR-GLS, the performance is significantly improved for DP-MP, especially for the large deformation.

Similarly, Table 3-10 show the mean and standard deviation ($\mu \pm \sigma$) of the registration errors of seven methods, when the model point set is wrapped by outlier, occlusion, rotation, and noise, respectively. We can see that the mean registration errors of DP-MP are lower than that of other methods for most sequences. Moreover, the standard deviations of DP-MP are generally smaller than that of other methods. Therefore, compared to other methods, DP-MP is more accurate and robust for the various synthetic data of the shapes fish and Fu.

For Table 6, the registration error of DP-MP is larger than that of MR when the occlusion percentage P_{oc} is set as 0.5. As the topology structure of Fu is relative complex, the target points may be easily matched wrong when the occlusion percentage P_{oc} is relative large for the membership probability representations of DP-MP and PR-GLS. In MR, the manifold regularization term is utilized to enforce a global structure constraint on the likelihood. Therefore, the effect of occlusion can be alleviated effectively.

2) EXPERIMENTAL RESULTS ON THREE IRREGULAR SHAPES

We also present the experimental results on three irregular shapes [8], as shown in Fig. 5. Table 11 shows the registration errors of the seven methods for three irregular shapes. We can see that the proposed method can achieve the best performance among the seven methods.

3) EXPERIMENTAL RESULTS ON 3D FACE IMAGES

Besides 2D data, we also performed the experimental comparisons on three sets of 3D face image sequences provided by the Bosphorus database [25], face recognition grand challenge (FRGC), and [16]. As an example, Fig. 6 shows the

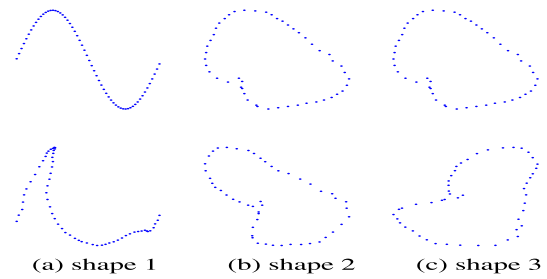


FIGURE 5. Model points (top row) and their corresponding target points (bottom row) for three irregular shapes.

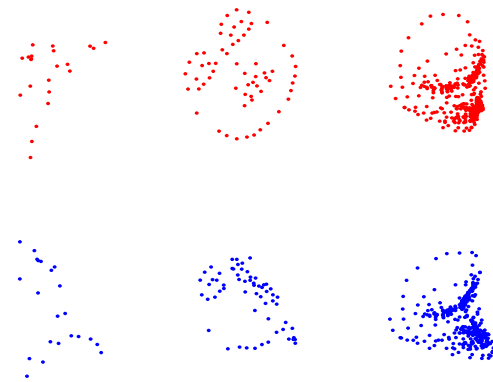


FIGURE 6. An example of model points (top row) and their corresponding target points (bottom row) of three 3D face images.

model points (top row) and their corresponding target points (bottom row) of three 3D face images. For each sequence, ten trials are carried out on ten frame pairs. Since shape context is used as a feature descriptor, MSTT can only deal

TABLE 5. The mean and standard deviation ($\mu \pm \sigma$) of the registration errors of seven methods when the occlusion percentage P_{oc} is set as different value for the *fish* point sets.

P_{oc}	0.1	0.2	0.3	0.4	0.5
MSTT	0.0022±0.0012	0.0038±0.0015	0.0109±0.0117	0.0114±0.0116	0.0181±0.0137
APM	0.0025±0.0009	0.0033±0.0016	0.0024±0.0011	0.0026±0.0013	0.0032±0.0017
CPD	1.4955e-4±3.6945e-4	7.7748e-4±6.6186e-4	0.0015±0.0008	0.0047±0.0012	0.0064±0.0015
PR-GLS	9.8250e-7±7.4425e-7	1.5779e-6±8.4338e-7	2.2219e-4±2.9391e-4	4.8414e-4±4.3363e-4	0.0017±9.7107e-4
SCGF	8.8194e-4±2.5455e-4	3.6204e-4±3.2145e-4	5.3790e-4±4.2703e-4	0.0028±0.0024	0.0039±0.0032
MR	3.4950e-5±6.0822e-5	3.3206e-4±5.4144e-4	0.0010±5.0269e-4	9.8793e-4±4.2080e-4	0.0013±7.9658e-4
DP-MP	9.8956e-7±9.1506e-7	1.0087e-6±9.2746e-7	3.6980e-5±1.1337e-4	1.4506e-4±3.2613e-4	3.3655e-4±5.4047e-4

TABLE 6. The mean and standard deviation ($\mu \pm \sigma$) of the registration errors of seven methods when the occlusion percentage P_{oc} is set as different value for the Chinese character *Fu*.

P_{oc}	0.1	0.2	0.3	0.4	0.5
MSTT	0.0041±0.0021	0.0054±0.0025	0.0104±0.01089	0.0226±0.0167	0.0252±0.0161
APM	0.0045±0.0013	0.0043±0.0024	0.0042±0.0022	0.0063±0.0085	0.0124±0.0169
CPD	4.1745e-4±2.7400e-4	0.0012±3.3026e-4	0.0020±0.0018	0.0099±0.0052	0.0127±0.0026
PR-GLS	0.0048±0.0031	0.0039±0.0015	0.0078±0.0038	0.0159±0.0042	0.0207±0.0042
SCGF	4.4371e-4±3.5483e-4	7.9009e-4±5.6439e-4	0.0029±0.0049	0.0053±0.0054	0.0053±0.0034
MR	2.3269e-4±4.1301e-4	7.3682e-4±1.2253e-4	0.0016±7.9283e-4	0.0029±7.5646e-4	0.0039±7.0052e-4
DP-MP	1.1614e-6±9.7404e-7	9.5377e-7±9.9029e-7	1.1658e-6±8.7009e-7	9.8070e-5±2.0279e-4	0.0041±0.0066

TABLE 7. The mean and standard deviation ($\mu \pm \sigma$) of the registration errors of seven methods when the rotation angle δ is set as different value for the *fish* point sets.

δ	-60	-30	0	30	60
MSTT	0.0017±0.0012	0.0016±0.0011	0.0017±0.0011	0.0017±0.0012	0.0017±0.0011
APM	0.0233±0.0091	0.0029±8.6617e-4	0.0015±0.0009	0.0025±0.0011	0.0155±0.0090
CPD	0.0241±0.0124	6.1054e-5±1.2622e-4	1.2169e-6±9.2278e-7	4.8385e-5±1.4365e-4	0.0116±0.0151
PR-GLS	0.0076±0.0104	2.8585e-6±2.4762e-6	1.1890e-6±8.4312e-7	2.7537e-5±7.5900e-5	0.0030±0.0094
SCGF	4.0772e-4±1.6916e-4	1.6298e-4±3.0265e-5	2.2301e-4±2.8584e-4	1.8189e-4±1.3072e-4	3.2608e-4±1.9915e-4
MR	0.0038±4.9147e-4	7.8502e-5±4.2626e-5	1.3849e-5±1.8468e-5	1.7686e-4±4.6487e-4	0.0042±6.5918e-4
DP-MP	2.2527e-6±1.0961e-6	1.0823e-6±6.1796e-7	1.0133e-6±9.6902e-7	1.5128e-6±1.0260e-6	2.2946e-6±3.0903e-6

TABLE 8. The mean and standard deviation ($\mu \pm \sigma$) of the registration errors of seven methods when the rotation angle δ is set as different value for the Chinese character *Fu*.

δ	-60	-30	0	30	60
MSTT	0.0028±0.0016	0.0027±0.0016	0.0027±0.0015	0.0028±0.0016	0.0027±0.0016
APM	0.0288±0.0093	0.0093±0.0073	0.0023±0.0015	0.0080±0.0078	0.0284±0.0059
CPD	0.0298±0.0146	7.6170e-5±2.3258e-4	1.5180e-6±1.0949e-6	0.0040±0.0101	0.0339±0.0053
PR-GLS	0.0244±0.0106	0.0026±0.0105	1.6778e-4±2.8677e-4	0.0043±0.0064	0.0233±0.0109
SCGF	5.8818e-4±2.2468e-4	3.7384e-4±2.2785e-4	5.7185e-4±5.5625e-4	3.1765e-4±2.2134e-4	6.7359e-4±4.6514e-4
MR	0.0048±7.3929e-4	0.0026±0.0026	2.3091e-5±2.6242e-5	0.0025±0.0026	0.0045±5.0859e-4
DP-MP	1.7463e-6±1.1426e-6	1.4818e-6±1.0516e-6	1.0456e-6±8.0857e-7	2.0889e-6±1.2461e-6	2.1533e-6±8.5264e-7

TABLE 9. The mean and standard deviation ($\mu \pm \sigma$) of the registration errors of seven methods when the noise percentage P_n is set as different value for the *fish* point sets.

P_n	0.01	0.02	0.03	0.04	0.05
MSTT	0.0018±0.0011	0.0053±0.0101	5.9408e-3±0.0099	6.7243e-3±0.0098	7.2824e-3±9.6227e-3
APM	0.0017±9.1871e-4	0.0019±8.3624e-4	2.2781e-3±7.4516e-4	2.6543e-3±6.9005e-4	3.0372e-3±6.1692e-4
CPD	4.5887e-4±2.9577e-5	9.3641e-4±6.1438e-5	1.4498e-3±6.7851e-5	1.9524e-3±1.0449e-4	2.4560e-3±1.5638e-4
PR-GLS	4.6317e-4±3.6170e-5	9.2928e-4±5.9420e-5	1.4021e-3±8.8859e-5	1.8698e-3±1.1350e-4	2.3555e-3±1.6020e-4
SCGF	6.1389e-4±2.5556e-4	9.5286e-4±1.4476e-4	1.3872e-3±1.3701e-4	1.9423e-3±4.8542e-4	2.3763e-3±4.8972e-4
MR	4.6007e-4±2.7865e-5	0.0010±1.6825e-4	1.5888e-3±2.1120e-4	1.9469e-3±2.0307e-4	2.3240e-3±1.9381e-4
DP-MP	4.5700e-4±3.1115e-5	9.1931e-4±5.7692e-5	1.3825e-3±8.5886e-5	1.8483e-3±1.1309e-4	2.3166e-3±1.4155e-4

with 2D data. Figure 7 shows the registration errors of six methods for three sequences, respectively. The registration errors of SCGF are significantly larger than that of other

methods. For easier comparison, the logarithm of the registration error is adopted as the longitudinal coordinate. Moreover, Table 14 tabulates the corresponding mean and standard

TABLE 10. The mean and standard deviation ($\mu \pm \sigma$) of the registration errors of seven methods when the noise percentage P_n is set as different value for the Chinese character Fu.

P_n	0.01	0.02	0.03	0.04	0.05
MSTT	0.0028±0.0015	0.0033±0.0015	4.2376e-3±1.8726e-4	4.6806e-3±2.1988e-3	5.6233e-3±2.0756e-3
APM	0.0024±0.0014	0.0026±0.0013	2.9287e-3±1.2341e-3	3.2729e-3±1.1572e-3	3.6476e-3±1.0872e-3
CPD	4.7267e-4±3.8026e-5	9.6055e-4±7.6284e-5	1.4799e-3±1.1864e-4	2.0313e-3±1.3919e-4	2.5687e-3±1.2768e-4
PR-GLS	6.3568e-4±3.2420e-4	0.0010±2.3046e-4	1.5006e-3±1.4373e-4	2.0337e-3±1.7492e-4	2.5483e-3±1.9039e-4
SCGF	7.3390e-4±2.7919e-4	0.0012±2.6355e-4	1.6238e-3±4.5728e-4	1.9920e-3±1.9741e-4	2.5381e-3±3.0649e-4
MR	4.7785e-4±4.1656e-5	9.5621e-4±6.9243e-5	1.4501e-3±1.2168e-4	1.9513e-3±1.6691e-4	2.4412e-3±2.1531e-4
DP-MP	4.7288e-4±3.7405e-5	9.5568e-4±7.2718e-5	1.4419e-3±1.0681e-4	1.9314e-3±1.4037e-4	2.4237e-3±1.7376e-4

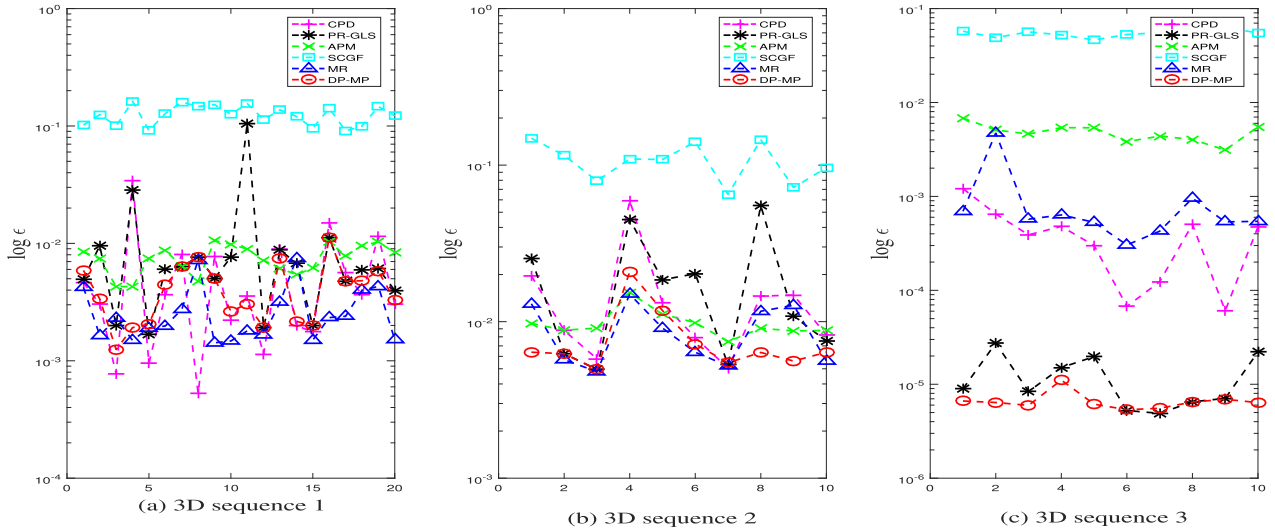


FIGURE 7. The registration errors of six methods for three 3D sequences.

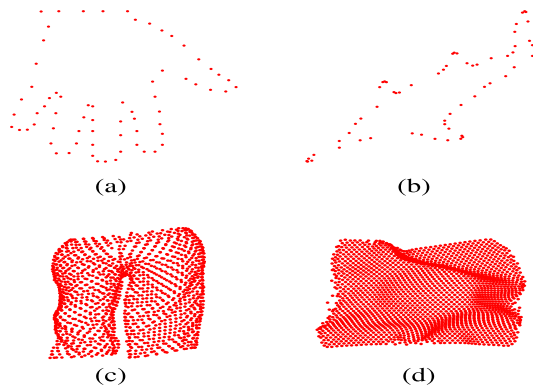


FIGURE 8. Three types of more complex point sets, 2D contour-like shapes (a: hand, b: fish), 3D surface-like shape (c: pace), and 3D cloud-like shape (d: coin).

deviation ($\mu \pm \sigma$) of the registration errors. We can see from Fig. 7 and Table 14 that, the registration errors of MR and DP-MP are obviously smaller than that of other methods. For 3D shape 1, the point number is only 22, which is far less than that of other data. The performance of DP algorithm is significantly affected when the point number is very small. Thus, the registration error of DP-MP is larger than that of MR.

TABLE 11. The registration errors (ϵ) of seven methods for three irregular shapes.

Shape	1	2	3
MSTT	0.088952	0.006404	0.006452
APM	0.013272	0.006386	0.025691
CPD	0.006344	0.004281	0.024825
PR-GLS	0.001412	0.000922	0.029344
SCGF	0.003149	0.002796	0.002046
MR	0.002080	0.001468	0.006044
DP-MP	0.001405	0.000922	0.001735

4) EXPERIMENTAL RESULTS ON THE POINT SETS OF 2D CONTOUR-LIKE SHAPES (HAND, FISH), 3D CLOUD-LIKE SHAPE (PACE), AND 3D SURFACE-LIKE SHAPE (COIN).

As shown in Fig. 8, three types of more complex point sets, 2D contour-like shapes (hand, fish), 3D cloud-like shape (pace), and 3D surface-like shape (coin), are adopted to compare the performance of the various methods. Table 13 shows the registration errors of 2D contour-like shape hand and fish. We can see that the registration errors of MR and DP-MP are less than that of other methods. In MR, the manifold regularization term can better capture the global structure of the 2D contour-like shape. Therefore, the registration error of MR is lower than that of DP-MP.

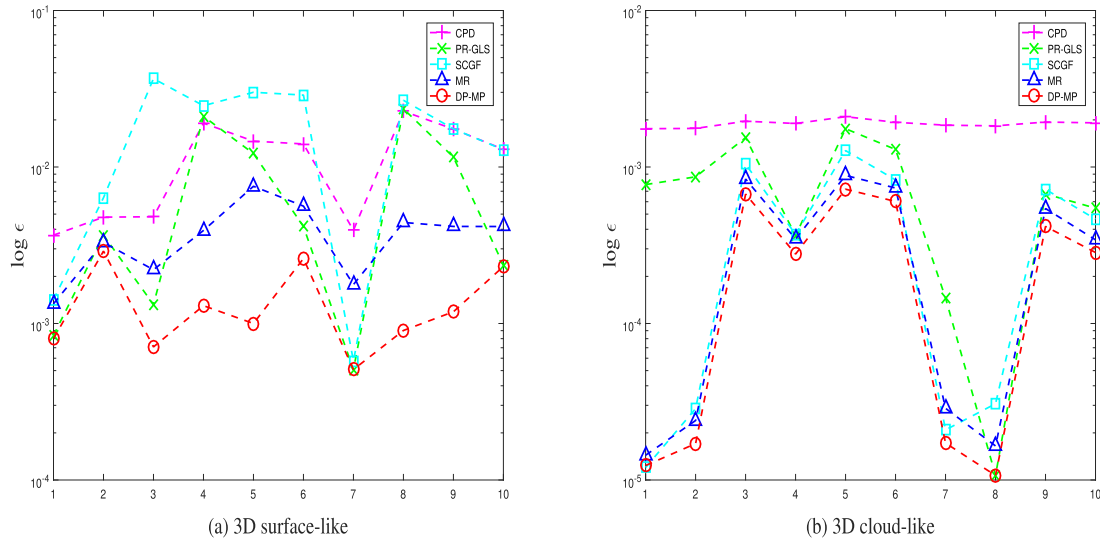


FIGURE 9. The registration errors of five methods for 3D sequence pace and coin.

TABLE 12. The mean and standard deviation ($\mu \pm \sigma$) of the registration errors of six methods for three 3D sequences.

Sequence	APM	CPD	PR-GLS	SCGF	MR	DP-MP
1	0.007620±0.002022	0.006097±0.007662	0.011799±0.022751	0.125835±0.023769	0.002817±0.001783	0.004347±0.002517
2	0.009802±0.002150	0.015715±0.015984	0.019885±0.017476	0.108028±0.030303	0.008917±0.003854	0.008116±0.004850
3	0.004820±0.001049	4.2599e-4±3.4099e-4	1.2527e-5±8.0107e-6	0.004732±0.053865	9.9381e-4±0.004732	6.6875e-6±1.6149e-6

TABLE 13. The registration errors of 2D contour-like shape hand and fish.

Shape	MSTT	APM	CPD	PR-GLS	SCGF	MR	DP-MP
hand	0.0306	0.0251	0.0250	0.0259	0.0238	0.0145	0.0223
fish	0.0511	0.0539	0.0472	0.0492	0.0498	0.0103	0.0397

Figure 9 shows the registration errors of five methods for 3D sequence pace and coin. Correspondingly, Table 14 tabulates the mean and standard deviation ($\mu \pm \sigma$) of the registration errors. Compared to other methods, we can see that DP-MP can achieve the best performance.

C. RELATED DISCUSSIONS

1) THE EFFECTIVENESS OF THE MEMBERSHIP PROBABILITY REPRESENTATION

In order to investigate the effectiveness of proposed membership probability representation C_{mm} and the DP algorithm, we conducted the experiments to evaluate the performance for four cases, i.e., (a) the original PR-GLS algorithm, (b) initial membership probability with the proposed representation C_{mm} , and used as the input of PR-GLS, denoted as MP+PR-GLS, (c) search for the optimal candidate points

with DP for the original membership probability representation of PR-GLS, denoted as DP+PR-GLS, (d) the proposed approach, i.e., DP-MP.

Take the synthetic data from *Fu* for example, Table 15-17 shows the registration errors of four cases when the deformation parameter β , the occlusion percentage P_{oc} , and the rotation angle δ , are set as different values. Compared to PR-GLS, the registration errors generally can be decreased by adopting the new membership probability representation or the DP algorithm.

2) COMPLEXITY ANALYSIS

Referring to [26], the computational complexity is roughly analyzed by considering the costs of updating the objective function and the unknown parameters. For DP-MP, the computational complexities of the membership probability assignment and the objective function are $O(N^3)$ and $O(N^2M + N^3)$. Thus, the total computational complexity of DP-MP is $O(N^2M + N^3)$. As the related methods, the computational complexities of CPD, PR-GLS, and MR are $O(M^2N + M^3)$, $O(N^2M + N^3)$, $O(M^2N + M^3)$, respectively. Therefore, the computational complexities of the four methods are close to each other.

TABLE 14. The mean and standard deviation ($\mu \pm \sigma$) of the registration errors of five methods for two 3D cloud-like shapes pace and coin.

Sequence	CPD	PRGLS	SCGF	MR	DP-MP
pace	0.011809±0.007029	0.008125±0.008565	0.018563±0.012771	0.003845±0.001852	0.001422±0.000857
coin	0.001893±0.000101	0.000797±0.000580	0.000479±0.000468	0.000377±0.000355	0.000303±0.000288

TABLE 15. The registration errors of four cases for the synthetic data from F_u when the deformation parameter β is set as different values.

β	0.04	0.06	0.08	0.10	0.12
PR-GLS	1.6778e-4	6.9188e-4	1.8302e-3	4.0312e-3	7.2048e-3
MP+PR-GLS	1.1824e-6	1.4834e-6	2.4726e-6	1.7032e-6	2.4085e-6
DP+PR-GLS	1.6763e-4	6.9029e-4	1.6639e-3	2.2559e-3	5.9315e-3
DP-MP	1.0456e-6	1.1873e-6	1.9412e-6	2.0358e-6	2.3445e-6

TABLE 16. The registration errors of four cases for the synthetic data from F_u when the occlusion percentage P_{oc} is set as different values.

P_{oc}	0.1	0.2	0.3	0.4	0.5
PR-GLS	0.004814	0.003863	0.007762	0.015956	0.020724
MP+PR-GLS	9.0955e-7	5.9921e-4	0.001174	0.002320	0.006882
DP+PR-GLS	0.002231	0.003228	0.006422	0.014506	0.020701
DP-MP	1.1614e-6	9.5377e-7	1.1658e-6	9.8070e-5	0.004139

TABLE 17. The registration errors of four cases for the synthetic data from F_u when the rotation angle δ is set as different values.

δ	-60	30	0	30	60
PR-GLS	0.024436	0.005581	1.6778e-4	0.004347	0.023311
MP+PR-GLS	0.016131	1.9538e-6	1.1824e-6	1.3995e-6	0.012793
DP+PR-GLS	0.014751	7.5053e-4	1.6763e-4	0.002680	0.014561
DP-MP	1.7463e-6	1.4818e-6	1.0456e-6	2.0889e-6	2.1534e-6

TABLE 18. The average running time (second).

Method	MSTT	APM	CPD	PR-GLS	SCGF	MR	DP-MP
time	1.9791	0.9643	1.0257	0.7469	45.6008	1.1350	1.6984

Furthermore, take one synthetic data of fish for example, Table 18 shows the run times of the various methods. The run time of SCGF is significantly larger than that of the other five methods. Nevertheless, the run-times are close to each other for other methods.

3) ANALYSIS OF CONVERGENCE

Similar to [17], a global optimum solution cannot be derived via the optimization process, because the objective function (2) is also not convex. As done in [17], the variance σ^2 is initialized with a large value in the EM algorithm. As a result, a lot of unstable shallow local minima can be filtered out, because the objective function becomes convex in a large region. In practice, a stable local minimum may be sufficient in many applications. In experiments, similar to [17], the iteration is terminated when the difference of transformation $T(\mathbf{x})$ of two successive iterations is less than a given threshold.

IV. CONCLUSION

In this paper, two strategies, i.e., a new representation for membership probability of Gaussian mixture model, and a dynamic programming algorithm, are proposed to improve the robustness of point set registration. Experimental results on some widely used data sets demonstrated that, compared to state-of-the-art approaches, a better comprehensive performance can be achieved by the proposed approach.

REFERENCES

- [1] C. Yang, Y. Liu, X. Jiang, Z. Zhang, L. Wei, T. Lai, and R. Chen, "Non-rigid point set registration via adaptive weighted objective function," *IEEE Access*, vol. 6, pp. 75947–75960, 2018.
- [2] J. Ma and J. Zhao, "Robust topological navigation via convolutional neural network feature and sharpness measure," *IEEE Access*, vol. 5, pp. 20707–20715, 2017.
- [3] S. Zhang, B. Li, F. Ren, and R. Dong, "High-precision measurement of binocular telecentric vision system with novel calibration and matching methods," *IEEE Access*, vol. 7, pp. 54682–54692, 2019.
- [4] H. Sang, Q. Wang, and Y. Zhao, "Multi-scale context attention network for stereo matching," *IEEE Access*, vol. 7, pp. 15152–15161, 2019.
- [5] C. Liao, W. Wang, K. Sakurada, and N. Kawaguchi, "Image-matching based identification of store signage using Web-crawled information," *IEEE Access*, vol. 6, pp. 45590–45605, 2018.
- [6] H. Chen, Y. Cui, R. Qiu, P. Chen, W. Liu, and K. Liu, "Image-alignment based matching for irregular contour defects detection," *IEEE Access*, vol. 6, pp. 68749–68759, 2018.
- [7] Z. Zhang, "Iterative point matching for registration of free-form curves and surfaces," *Int. J. Comput. Vis.*, vol. 13, no. 2, pp. 119–152, Oct. 1994.
- [8] H. Chui and A. Rangarajan, "A new point matching algorithm for non-rigid registration," *Comput. Vis. Image Understand.*, vol. 89, nos. 2–3, pp. 114–141, Feb. 2003.
- [9] W. Lian, L. Zhang, and M.-H. Yang, "An efficient globally optimal algorithm for asymmetric point matching," *IEEE Trans. Pattern Anal. Mach. Intell.*, vol. 39, no. 7, pp. 1281–1293, Jul. 2017.
- [10] S. Belongie, J. Malik, and J. Puzicha, "Shape matching and object recognition using shape contexts," *IEEE Trans. Pattern Anal. Mach. Intell.*, vol. 24, no. 4, pp. 509–522, Apr. 2002.
- [11] J. Tang, L. Shao, X. Li, and K. Lu, "A local structural descriptor for image matching via normalized graph Laplacian embedding," *IEEE Trans. Cybern.*, vol. 46, no. 2, pp. 410–420, Feb. 2016.
- [12] Y. Yang, S. H. Ong, and K. W. C. Foong, "A robust global and local mixture distance based non-rigid point set registration," *Pattern Recognit.*, vol. 48, no. 1, pp. 156–173, Jan. 2015.
- [13] Y. Tsin and T. Kanade, "A correlation-based approach to robust point set registration," in *Proc. Eur. Conf. Comput. Vis.*, 2004, pp. 558–569.
- [14] T. M. Nguyen and Q. M. J. Wu, "Multiple kernel point set registration," *IEEE Trans. Med. Imag.*, vol. 35, no. 6, pp. 1381–1394, Jun. 2016.
- [15] B. Jian and B. C. Vemuri, "Robust point set registration using Gaussian mixture models," *IEEE Trans. Pattern Anal. Mach. Intell.*, vol. 33, no. 8, pp. 1633–1645, Aug. 2011.
- [16] A. Myronenko and X. Song, "Point set registration: Coherent point drift," *IEEE Trans. Pattern Anal. Mach. Intell.*, vol. 32, no. 12, pp. 2262–2275, Dec. 2010.
- [17] J. Ma, J. Zhao, and A. L. Yuille, "Non-rigid point set registration by preserving global and local structures," *IEEE Trans. Image Process.*, vol. 25, no. 1, pp. 53–64, Jan. 2016.
- [18] P. F. Felzenszwalb and R. Zabih, "Dynamic programming and graph algorithms in computer vision," *IEEE Trans. Pattern Anal. Mach. Intell.*, vol. 33, no. 4, pp. 721–740, Apr. 2011.
- [19] R. B. Rusu, N. Blodow, and M. Beetz, "Fast point feature histograms (FPFH) for 3D registration," in *Proc. IEEE Int. Conf. Robot. Autom.*, May 2009, pp. 3212–3217.
- [20] W. Lian, L. Zhang, and D. Zhang, "Rotation-invariant nonrigid point set matching in cluttered scenes," *IEEE Trans. Image Process.*, vol. 21, no. 5, pp. 2786–2797, May 2012.
- [21] G. Wang, Q. Zhou, and Y. Chen, "Robust non-rigid point set registration using spatially constrained Gaussian fields," *IEEE Trans. Image Process.*, vol. 26, no. 4, pp. 1759–1769, Apr. 2017.
- [22] J. Ma, J. Zhao, J. Jiang, and H. Zhong, "Non-rigid point set registration with robust transformation estimation under manifold regularization," in *Proc. AAAI Conf. Artif. Intell.*, 2017, pp. 4218–4224.
- [23] J. Ma, J. Wu, J. Zhao, J. Jiang, H. Zhou, and Q. Z. Sheng, "Nonrigid point set registration with robust transformation learning under manifold regularization," *IEEE Trans. Neural Netw. Learn. Syst.*, vol. 30, no. 12, pp. 3584–3597, Dec. 2019, doi: 10.1109/tnnls.2018.2872528.
- [24] M. Lee, J. Cho, C. H. Choi, and S. Oh, "Procrustean normal distribution for non-rigid structure from motion," in *Proc. IEEE Conf. Comput. Vis. Pattern Recognit.*, Jun. 2013, pp. 1280–1287.
- [25] A. Savran, N. Alyüz, H. Dibeklioğlu, O. Çliktutan, B. G. O. Berk, B. Sankur, and L. Akarun, "Bosphorus database for 3D face analysis," in *Proc. 1st COST 2101 Workshop Biometrics Identity Manage.*, May 2008.

- [26] J. Ma, W. Qiu, J. Zhao, Y. Ma, A. L. Yuille, and Z. Tu, "Robust L_2E estimation of transformation for non-rigid registration," *IEEE Trans. Signal Process.*, vol. 63, no. 5, pp. 1115–1129, Mar. 2015.



LU-JIE FANG is currently pursuing the master's degree with the School of Electrical Engineering and Automation, Anhui University. Her research interests include machine learning, and image and signal processing.



ZHAN-LI SUN (Member, IEEE) received the Ph.D. degree from the University of Science and Technology of China, in 2005.

Since 2006, he has worked with The Hong Kong Polytechnic University, Nanyang Technological University, and the National University of Singapore. He is currently a Professor with the School of Electrical Engineering and Automation, Anhui University, China. His research interests include machine learning, and image and signal processing.

He serves as an Associate Editor of IEEE Access.



KIN-MAN LAM (Senior Member, IEEE) received the Associate degree (Hons.) in electronic engineering from The Hong Kong Polytechnic University (formerly called Hong Kong Polytechnic), in 1986, the M.Sc. degree in communication engineering from the Department of Electrical Engineering, Imperial College of Science, Technology and Medicine, London, U.K., in 1987, and the Ph.D. degree from the Department of Electrical Engineering, The University of Sydney, Sydney,

Australia, in August 1996.

From 1990 to 1993, he was a Lecturer with the Department of Electronic Engineering, The Hong Kong Polytechnic University. He joined the Department of Electronic and Information Engineering, The Hong Kong Polytechnic University, as an Assistant Professor, in October 1996, became an Associate Professor, in 1999, and has been a Professor, since 2010. His current research interests include human face recognition, image and video processing, and computer vision. He has been a member of the organizing committee and program committee of many international conferences. He is a BoG Member of the Asia-Pacific Signal and Information Processing Association (APSIPA) and the Director-Student Services of the IEEE Signal Processing Society. He is currently a General Co-Chair of the IEEE International Conference on Signal Processing, Communications, and Computing (ICSPCC2012). He also serves as an Associate Editor of the IEEE TRANSACTIONS ON IMAGE PROCESSING, the *APSIPA Transactions on Signal and Information Processing*, and the *EURASIP International Journal on Image and Video Processing*.

• • •